DOI: 10.1002/ ((please add manuscript number))
Article type: Full Paper

K-ion batteries based on a P2-type $K_{0.6}CoO_2$ cathode

*Haegyeom Kim, Jae Chul Kim, Shou-Hang Bo, Tan Shi, Gerbrand Ceder**

Dr. H. Kim, Dr. J. C. Kim, Dr. S. –H. Bo
Materials Sciences Division, Lawrence Berkeley National Laboratory, Berkeley, CA 94720, USA
T. Shi, Prof. G. Ceder*
Department of Materials Science and Engineering, University of California, Berkeley, CA 94720, USA
E-mail: gceder@berkeley.edu

Keywords: potassium, batteries, energy storage, cobalt oxide, cathode

K-ion batteries are a potentially exciting and new energy storage technology that can combine high specific energy, cycle life, and good power capability, all while using abundant potassium resources. The discovery of novel cathodes is a critical step toward realizing K-ion batteries (KIBs). In this work, we develop a layered P2-type $K_{0.6}CoO_2$ cathode and demonstrate highly reversible K ion intercalation. *In situ* X-ray diffraction combined with electrochemical titration reveals that P2-type $K_{0.6}CoO_2$ can store and release a considerable amount of K ions *via* a topotactic reaction. Despite the large amount of phase transitions as function of K content, the cathode operates highly reversibly and with good rate capability. We further demonstrate the practical feasibility of KIBs by constructing full cells with a graphite anode. This work highlights the potential of KIBs as viable alternatives for Li-ion and Na-ion batteries and provides new insights and directions for the development of next-generation energy storage systems.

1. Introduction

Electrochemical energy storage has enriched our daily life by enabling the mobile devices which have spawned novel ways of conducting business and personal transactions. The growth of Li-ion batteries into novel applications such as electric vehicles and grid, for which

it was not originally designed, has spurred considerably research into alternative, more cost-effective chemistries, including Na and Mg-ion based systems. These chemistries have a less negative standard redox potential than Li, thereby lowering the operating voltage and decreasing energy density. From this perspective, K-ion cells would be a more reasonable choice as a low-cost alternative to Li-ion since K has high natural abundance and a lower standard redox potential than Na (K/K^+: -2.9 V and Na/Na^+: -2.7 V *vs.* saturated hydrogen electrode in aqueous media).[1] Indeed, the potential of K/K^+ was theoretically calculated to be even more negative than that of Li/Li^+ in propylene carbonate, a well-known battery electrolyte solvent.[2] Experimental demonstration that the standard redox potential of K/K^+ is lower than that of Li/Li^+ by ~0.15 V in ethylene carbonate/diethyl carbonate electrolyte is consistent with this prediction.[3] This interesting feature suggests that KIBs might potentially deliver a higher cell voltage than Na-ion batteries (NIBs) and even Li-ion batteries (LIBs). In addition, K-ion technology would benefit from the fact that graphite can be used on the anode side[3, 4] (as in Li-ion), which is not the case for Na-ion and has seriously limited application of Na-ion technology.

Only a few cathode compounds have been reported to date for KIBs,[5-9] with most studies focusing on the development of anodes.[3, 4, 10-20] For example, Eftekhari demonstrated that Prussian blue can reversibly store K ions in a non-aqueous electrolyte system.[5] Later, the amorphous phase of $FePO_4$ as well as organic materials were also suggested as cathodes for KIBs.[6-9] Recently K-ion insertion was shown to be possible in $K_{0.3}MnO_2$,[21] but the low K content of that material requires the use of K metal or pre-potassiated anodes.

In this paper, we demonstrate highly reversible cycling of a P2-type $K_{0.6}CoO_2$ cathode, and show implementation of a full cell K-ion battery using a graphite anode. Alkali transition metal oxides with an ordered rock-salt structure have been widely studied as promising cathodes for LIBs and NIBs because their layered framework allows topotactic de/intercalation of alkali ions, leading to excellent energy storage properties.[22-28] Cyclability

and rate capability of the K_xCoO_2 are shown to be very good, indicating that with further improvements K-ion may be an effective technology for large-scale energy storage. To the best of our knowledge, this is the first demonstration of reversible K de/intercalation in P2-type layered K_xCoO_2 in the range $0.33 < x < 0.68$. This work creates new research opportunities for the development of KIBs as a particularly exciting and promising technology for large-scale energy storage applications.

2. Results

2.1. Structure of as-synthesized $K_{0.6}CoO_2$

Figure 1a shows the Rietveld-refined profile of an X-ray diffraction (XRD) pattern obtained from as-synthesized $K_{0.6}CoO_2$ that was prepared by a conventional solid-state route (see Methods). The full pattern matching result indicates hexagonal symmetry with a P63/mmc space group. The lattice parameters were determined to be $a = b = 2.838$ Å and $c = 12.372$ Å, which agrees well with the results previously reported in the literature (Figure 1a).[29] These parameters correspond to a P2-type layered structure, as illustrated in Figure 1b. The scanning electron microscopy (SEM) image in the inset of Figure 1a indicates that the average particle size is ~2.5 μm. Inductively coupled plasma-mass spectroscopy analysis further confirms that the K:Co ratio in the sample is approximately 0.61:1.0. Note that using solid-state methods, K_xCoO_2 with a P2-type structure can be only synthesized for $0.5 < x < 0.6$.[30] In contrast, P2-type Na_yCoO_2 can contain a large amount of Na ($y \approx 0.74$).[31] This difference may be caused by the larger size of K^+ ion compared with that of Na^+, which will be further discussed later.

2.2. Reversible K-ion extraction and reinsertion in $K_{0.6}CoO_2$

Figure 2 presents the first and second galvanostatic charge and discharge profiles of the P2-type $K_{0.6}CoO_2$ cathode at a current rate of 2 mA g^{-1} (C/16, 1 C = 80 mA g^{-1}). We obtain 62

and 80 mAh g^{-1} in the first charge and discharge, respectively, with an average voltage of ~2.7 V (*vs.* K/K^+), indicating that the effective K content can be varied between 0.33 and 0.68. The charge and discharge profiles are very similar, implying highly reversible K-ion intercalation and deintercalation processes. The dQ/dV derivative curves and enlarged charge/discharge profiles (inset (i) and (ii) of Figure 2) demonstrate a multitude of first-order phase transitions upon K extraction and insertion, even more than in P2-type Na_xCoO_2.[31]

To better understand the K-ion de/intercalation mechanisms in P2-type K_xCoO_2, we performed *in situ* XRD during electrochemical cycling (**Figure 3a**). We examined the (002), (004) and (008) diffraction peaks, which are most sensitive to the K content. Note that in Figure 3b, peaks other than (00*l*) are difficult to analyze because of the preferred orientation during electrode preparation, and the double peaks are due to Mo-Kα_2 radiation. Among the (00*l*) peaks, shifting of the (008) peak is the most noticeable upon K extraction and reinsertion, as observed in Figure 3c– Figure 3e. Upon charging, the (008) peak shifts to lower angles while the P2-type structure is preserved, as observed in Figure 3d. This result, commonly observed in layered A_xMO_2 (A: alkali metal, M: transition metal) compounds, indicates increasing inter-slab distances due to the increased repulsion between oxygens upon alkali ion deintercalation.[31-33] We also observe different degrees of shifting and asymmetric peak evolutions, which provides further evidence of a multitude of phase transitions in K_xCoO_2 as K ions are extracted. These phase transitions likely originate from K^+/vacancy ordering. To our knowledge, this multitude of reversible phase transitions is unparalleled in any intercalation system. The *c* lattice parameters refined using the P2 structural model is plotted in Figure 3f. The overall trend is a continuous increase and decrease of the *c* lattice parameters upon charge and discharge, respectively. The 0.35 K difference between the charged and discharged states causes a change in *c* lattice parameter of ~3.5%, which is similar to that in the P2-type Na_xCoO_2 system (~4% expansion along the *c*-axis from 0.45 Na deintercalation).[34] These results clearly demonstrate that P2-type $K_{0.6}CoO_2$ can store K ions

via a highly reversible topotactic reaction, which is an essential factor for KIB cathode materials.

2.3. Rate capability and cycling of $K_{0.6}CoO_2$

Figure 4a and Figure 4b show the electrochemical performance of the P2-type $K_{0.6}CoO_2$ cathode at various rates ranging from 2 mA g^{-1} (C/40) to 150 mA g^{-1} (1.875 C). Discharge capacities of 78, 70, 66, 59, 48, and 43 mAh g^{-1} were obtained at 2, 10, 70, 100, 120, and 150 mA g^{-1}, respectively. The P2-type $K_{0.6}CoO_2$ cathode also exhibited good cyclability, maintaining reversible discharge capacities over multiple cycles at each rate. We further performed extended cycle stability measurements at a current rate of 100 mA g^{-1} (1.25 C), as shown in Figure 4c and Figure 4d. The P2-type $K_{0.6}CoO_2$ cathode retained ~60% of its initial capacity after ~120 cycles with a coulombic efficiency of ~99%. We observed that the shapes of the charge/discharge profiles were not significantly altered during repeated battery operations indicating that the cathode crystal structure remains well ordered (Figure S 1). The *ex situ* XRD results presented in Figure S 2, further confirm that repeated electrochemical cycling does not significantly affect the crystallinity of the P2-type $K_{0.6}CoO_2$ cathode. The diffraction patterns of the P2-type $K_{0.6}CoO_2$ cathodes after the 1^{st} and 50^{th} cycles are identical, and their full width at half maximum values, which represents the crystalline size, strain, and crystallinity, are almost unchanged. Hence, it seems unlikely that capacity loss is due to degradation of the cathode material. To eliminate the effect of the K metal anode and electrolyte stability on cycle life, we disassembled the coin-cell after ~120 cycles, replenished it with a fresh K metal anode and electrolyte, and then reassembled the cell. After this treatment, some of the capacity was recovered, as observed in Figure 4c. The shape of the charge and discharge voltage curves did not change (Figure S 3), indicating that the re-assembly did not affect the K de/intercalation reactions in P2-type $K_{0.6}CoO_2$. Thus, the side

reactions between the electrolyte and the K metal anode are likely responsible for at least some part of the capacity degradation.

2.4. Full cell demonstration of the $K_{0.6}CoO_2$ cathode with a graphite anode

To evaluate the practical feasibility of K-batteries, we tested the full cell performance of the $K_{0.6}CoO_2$ cathode with a graphite anode (**Figure 5**). The graphite anode was cycled between 0.01 and 1.5 V (*vs.* K/K^+) before the full cell assembly because of the large irreversible capacity in the first discharge process shown in Figure S 4. The full cell delivered a specific discharge capacity of ~53 mAh $g^{-1}_{cathode}$ at a rate of 3 mA g^{-1} Note that a full cell was assembled with the $K_{0.6}CoO_2$ cathode without pre-potassiation. Thus, the theoretical capacity was ~60 mAh $g^{-1}_{cathode}$ (K_xCoO_2, $0.6 < x < 0.33$) in this test. The full cell was capable of performing multiple K de/intercalation processes with the capacity decreasing gradually upon cycling (inset of Figure 5). The capacity decay can likely be attributed to the low coulombic efficiency of the graphite anode (~70 %), as shown in Figure S 4. This is not surprising given that the electrolyte was not optimized for use with K systems. Li-ion systems today contain a highly tuned set of additives to passivate the graphite anode after a few cycles. Although the electrochemical properties of the full cell require further improvement for practical use, our results demonstrate the potential of KIBs as viable alternatives for energy storage systems. We believe that by further optimizing the electrode compositions and chemistries as well as other critical components such as the anode, separator, and electrolyte, we can improve the practicality of this new system.

3. Discussion

In this paper, we demonstrate for the first time K^+ cycling in an intercalation oxide and the operation of a full-cell K-ion battery. The cycling of K in and out of K_xCoO_2 shows a remarkable amount of phase transitions, but despite this multitude of transitions, the cycling is

highly reversible. It is worth studying the difference with Na^+ intercalation in the P2 structure or Li^+ intercalation in O3 Li_xCoO_2, one of the most used LIB materials. In general, the voltage slope of the intercalation curves increases from Li to Na to K. Similarly, the number of observed phase transition features in the voltage curve increases in the same order. These trends are the consequence of the strengthening of the effective alkali-alkali interaction which is responsible for both the alkali ordering and the voltage slope.[35] Two factors contribute to this. Larger ionic size in general causes stronger effective interactions.[36] But, the dominant physics is probably the larger slab space as the alkali size increases from Li^+ to K^+. Screening of electrostatics between the alkali ions by oxygen strongly reduces their effective interaction,[35] and in the case of Li_xCoO_2 only a few weak order/disorder transitions occur. For the very large K^+ ion, the oxygen layers across the intercalating slab are much farther apart and only weakly screen the $K^+ – K^+$ repulsion, leading to a much larger effective interaction. Hence, the remarkable amount of phase transition features in the voltage curve (Figure 2). The larger slope of the voltage curve (Figure S 5) leads to a narrower intercalation range for K in P2-type K_xCoO_2 (0.33–0.68 between 1.7 and 4.0 V) than for Na in P2-type Na_yCoO_2 (0.35 and 0.87 between 2.0–3.8 V)[31]. Hence, less sloping voltage profiles for K insertion may be sought in systems with better screening such as sulfides and poly-anion systems.

The electrochemical properties, including the rate capability and cycle stability (Figure 4), of P2-type $K_{0.6}CoO_2$ are remarkable when considering its large particle size (> ~2 μm) without any further treatment or optimization. It is likely that the P2-type host structure can better maintain its structural stability upon electrochemical cycling compared to other types of compounds,[31, 37] leading to better cyclability. In addition, K ions in this P2-type structure can rapidly diffuse between the adjacent prismatic sites by direct hopping through the face-sharing facets.[25, 37-40] In comparison, for O3-type compounds, alkali ions in the octahedral sites migrate *via* face-sharing tetrahedral sites, which has a higher activation barrier due to the

strong electrostatic repulsion between the alkali ion in the tetrahedral site and metal ion in the MO_6 layers.[39]

4. Conclusion

We proposed a layered P2-type $K_{0.6}CoO_2$ as a new cathode for KIBs. This new cathode material can provide a reversible capacity of ~80 mAh g^{-1} with the K content in K_xCoO_2 varying between 0.33 and 0.68 and an average redox potential of ~2.7 V (*vs.* K/K^+). Multiple phase transitions during reversible K de/intercalation were observed, which likely originate from strong K^+/vacancy ordering. By combining *in situ* XRD analysis and electrochemical titration, we demonstrated that the overall P2-type structure is well preserved, indicating a reversible topotactic reaction. We also demonstrated the practical feasibility of KIBs by constructing a full cell consisting of a $K_{0.6}CoO_2$ cathode and graphite anode. This work will create new possibilities for the development of better-performing KIBs as next-generation energy storage systems.

5. Experimental Section

5.1. Synthesis of P2-type $K_{0.6}CoO_2$

The P2-type $K_{0.6}CoO_2$ was synthesized using a solid-state method. An excess amount (7 at%) of KOH (>90 %, Sigma Aldrich) was homogeneously mixed with Co_3O_4 (< 10 μm, Sigma–Aldrich) using a planetary ball-mill (Retsch PM200) at 300 rpm for 4 h. The resulting mixture was pelletized and fired at 600 ºC for 30 h under a flowing O_2 environment. After natural cooling, the temperature was held at 200 ºC before the samples were collected to prevent contamination from moisture in the air.

5.2. Characterization

The structure of $K_{0.6}CoO_2$ was analyzed using a Rigaku Miniflex 600 X-ray diffractometer with Cu Kα radiation. Structure analysis using Rietveld refinement was performed using

PANalytical HighScore Plus software. The morphology of the samples was verified by field-emission scanning electron microscopy (FE-SEM, Zeiss Gemini Ultra-55). *In situ* XRD was performed on a Bruker D8 Advance X-ray diffractometer equipped with Mo $K\alpha_1$ and α_2 radiation. The homemade *in situ* cell had a Be window and was galvanostatically cycled using a Solartron 1287 potentiostat.

5.3. Electrochemical test

Electrodes were prepared by mixing $K_{0.6}CoO_2$ (80 wt%), Super P carbon black (Timcal, 10 wt%), and dry polytetrafluoroethylene (DuPont, 10 wt%) in an Ar-filled glove box to prevent contamination from moisture. Coin cells (2032-type) were assembled in the glove box with a two-electrode configuration using K metal as a counter electrode. A separator of grade GF/F (Whatman, USA) and an electrolyte of 0.7 M KPF_6 in anhydrous EC/DEC solution (BASF, 1:1 volume ratio) were used. Cathode films with loading densities of ~6.76 mg cm^{-2} were electrochemically tested on an Arbin Instruments potentiostat. For the full cell test, a graphite anode was initially cycled between 0.01 and 1.5 V (*vs.* K/K^+) to remove the portion of irreversible capacity from the first cycle. The full cell was assembled with the $K_{0.6}CoO_2$ cathode and a graphite anode in a 2:1 weight ratio.

Supporting Information

Supporting Information is available from the Wiley Online Library or from the author.

Acknowledgements

The SEM experiments were performed at the Molecular Foundry, LBNL, supported by the Office of Science, Office of Basic Energy Sciences of the US Department of Energy (Contract No. DE-AC02-05CH11231).

Received: ((will be filled in by the editorial staff))
Revised: ((will be filled in by the editorial staff))
Published online: ((will be filled in by the editorial staff))

References

1. A. Eftekhari, Z. Jian and X. Ji, *ACS Appl. Mater. Interf.*, **2016**, DOI: 10.1021/acsami.1026b07989.
2. Y. Marcus, *Pure Appl. Chem.*, **1985**, *57*, 1129.
3. S. Komaba, T. Hasegawa, M. Dahbi and K. Kubota, *Electrochem. Commun.*, **2015**, *60*, 172-175.
4. Z. Jian, W. Luo and X. Ji, *J. Am. Chem. Soc.*, **2015**, *137*, 11566-11569.
5. A. Eftekhari, *J. Power Sources*, **2004**, *126*, 221-228.
6. V. Mathew, S. Kim, J. Kang, J. Gim, J. Song, J. P. Baboo, W. Park, D. Ahn, J. Han, L. Gu, Y. Wang, Y.-S. Hu, Y.-K. Sun and J. Kim, *NPG Asia Mater*, **2014**, *6*, e138.
7. Q. Zhao, J. Wang, Y. Lu, Y. Li, G. Liang and J. Chen, *Angew. Chem.*, **2016**, *128*, 12716-12720.
8. Y. Chen, W. Luo, M. Carter, L. Zhou, J. Dai, K. Fu, S. Lacey, T. Li, J. Wan, X. Han, Y. Bao and L. Hu, *Nano Energy*, **2015**, *18*, 205-211.
9. Z. Jian, Y. Liang, I. A. Rodríguez-Pérez, Y. Yao and X. Ji, *Electrochem. Commun.*, **2016**, *71*, 5-8.
10. W. Luo, J. Wan, B. Ozdemir, W. Bao, Y. Chen, J. Dai, H. Lin, Y. Xu, F. Gu, V. Barone and L. Hu, *Nano Lett.*, **2015**, *15*, 7671-7677.
11. Z. Jian, Z. Xing, C. Bommier, Z. Li and X. Ji, *Adv. Energy Mater.*, **2016**, *6*, 1501874.
12. J. Zhao, X. Zou, Y. Zhu, Y. Xu and C. Wang, *Adv. Funct. Mater.*, **2016**, *26*, 8103–8110
13. H. Kim, G. Yoon, K. Lim and K. Kang, *Chem. Commun.*, **2016**, *52*, 12618-12621.
14. A. P. Cohn, N. Muralidharan, R. Carter, K. Share, L. Oakes and C. L. Pint, *J. Mater. Chem. A*, **2016**, *4*, 14954-14959.
15. B. Kishore, V. G and N. Munichandraiah, *J. Electrochem. Soc.*, **2016**, *163*, A2551-A2554.
16. K. Share, A. P. Cohn, R. Carter, B. Rogers and C. L. Pint, *ACS Nano*, **2016**, *10*, 9738-9744.
17. Z. Ju, S. Zhang, Z. Xing, Q. Zhuang, Y. Qiang and Y. Qian, *ACS Appl. Mater. Interf.*, **2016**, *8*, 20682-20690.
18. I. Sultana, T. Ramireddy, M. M. Rahman, Y. Chen and A. M. Glushenkov, *Chem. Commun.*, **2016**, *52*, 9279-9282.
19. J. Han, M. Xu, Y. Niu, G.-N. Li, M. Wang, Y. Zhang, M. Jia and C. m. Li, *Chem. Commun.*, **2016**, *52*, 11274-11276.
20. J. Han, Y. Niu, S.-j. Bao, Y.-N. Yu, S.-Y. Lu and M. Xu, *Chem. Commun.*, **2016**, *52*, 11661-11664.
21. C. Vaalma, G. A. Giffin, D. Buchholz and S. Passerini, *J. Electrochem. Soc.*, **2016**, *163*, A1295-A1299.
22. H. Kim, H. Kim, Z. Ding, M. H. Lee, K. Lim, G. Yoon and K. Kang, *Adv. Energy Mater.*, **2016**, *6*, 1600943.
23. M. D. Slater, D. Kim, E. Lee and C. S. Johnson, *Adv. Funct. Mater.*, **2013**, *23*, 947-958.
24. P. He, H. Yu, D. Li and H. Zhou, *J. Mater. Chem.*, **2012**, *22*, 3680-3695.
25. R. J. Clément, P. G. Bruce and C. P. Grey, *J. Electrochem. Soc.*, **2015**, *162*, A2589-A2604.
26. M. Sathiya, G. Rousse, K. Ramesha, C. P. Laisa, H. Vezin, M. T. Sougrati, M. L. Doublet, D. Foix, D. Gonbeau, W. Walker, A. S. Prakash, M. Ben Hassine, L. Dupont and J. M. Tarascon, *Nat. Mater.*, **2013**, *12*, 827-835.

27. J.-Y. Hwang, S.-M. Oh, S.-T. Myung, K. Y. Chung, I. Belharouak and Y.-K. Sun, *Nat. Commun.*, **2015**, *6*, 6865.
28. Y.-N. Zhou, J. Ma, E. Hu, X. Yu, L. Gu, K.-W. Nam, L. Chen, Z. Wang and X.-Q. Yang, *Nat. Commun.*, **2014**, *5*, 5381.
29. M. Pollet, M. Blangero, J.-P. Doumerc, R. Decourt, D. Carlier, C. Denage and C. Delmas, *Inorg. Chem.*, **2009**, *48*, 9671-9683.
30. J. Sugiyama, Y. Ikedo, P. L. Russo, H. Nozaki, K. Mukai, D. Andreica, A. Amato, M. Blangero and C. Delmas, *Phys. Rev. B*, **2007**, *76*, 104412.
31. R. Journal of Power SourcesBerthelot, D. Carlier and C. Delmas, *Nat. Mater.*, **2011**, *10*, 74-80.
32. S.-H. Bo, X. Li, A. J. Toumar and G. Ceder, *Chem. Mater.*, **2016**, *28*, 1419-1429.
33. S. Komaba, N. Yabuuchi, T. Nakayama, A. Ogata, T. Ishikawa and I. Nakai, *Inorg. Chem.*, **2012**, *51*, 6211-6220.
34. J. J. Ding, Y. N. Zhou, Q. Sun, X. Q. Yu, X. Q. Yang and Z. W. Fu, *Electrochim. Acta*, **2013**, *87*, 388-393.
35. A. Van der Ven, M. K. Aydinol, G. Ceder, G. Kresse and J. Hafner, *Phys. Rev. B*, **1998**, *58*, 2975-2987.
36. D. D. Fontaine, in *Solid State Physics*, eds. F. S. Henry Ehrenreich and T. David, Academic Press, 1979, pp. 73-274.
37. S. Guo, Y. Sun, J. Yi, K. Zhu, P. Liu, Y. Zhu, G.-z. Zhu, M. Chen, M. Ishida and H. Zhou, *NPG Asia Mater*, **2016**, *8*, e266.
38. E. Lee, J. Lu, Y. Ren, X. Luo, X. Zhang, J. Wen, D. Miller, A. DeWahl, S. Hackney, B. Key, D. Kim, M. D. Slater and C. S. Johnson, *Adv. Energy Mater.*, **2014**, *4*, 1400458.
39. S. Guo, P. Liu, H. Yu, Y. Zhu, M. Chen, M. Ishida and H. Zhou, *Angew. Chem.*, **2015**, *127*, 5992-5997.
40. Y. Mo, S. P. Ong and G. Ceder, *Chem. Mater.*, **2014**, *26*, 5208-5214.

Figures

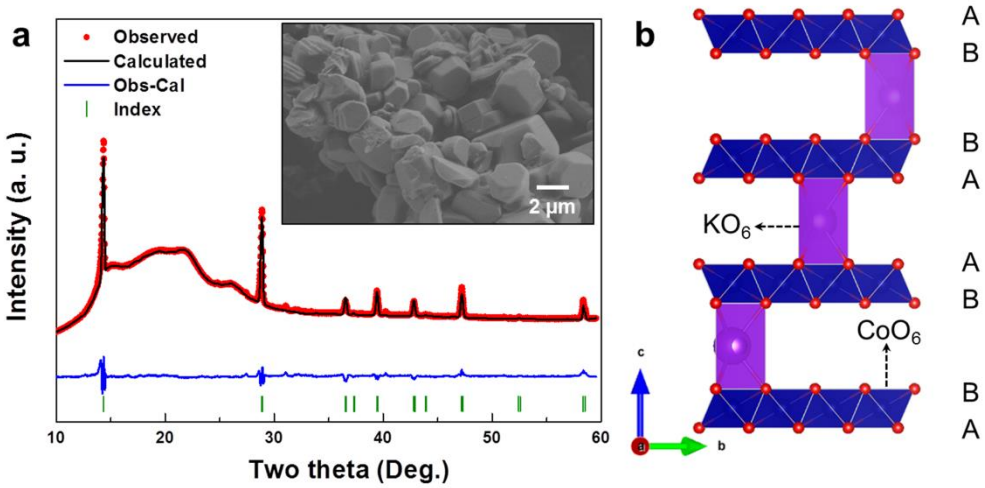

Figure 1. Structure characterization of P2-type $K_{0.6}CoO_2$. a. Full pattern matching of powder XRD for $K_{0.6}CoO_2$ sample (inset: SEM image). The broad background from 12° to 30º originates from the Kapton film used to seal the XRD sample. The refinement performed in the P63/mmc space group results in R_{wp} = 3.91. **b.** Schematic structure of P2-type $K_{0.6}CoO_2$.

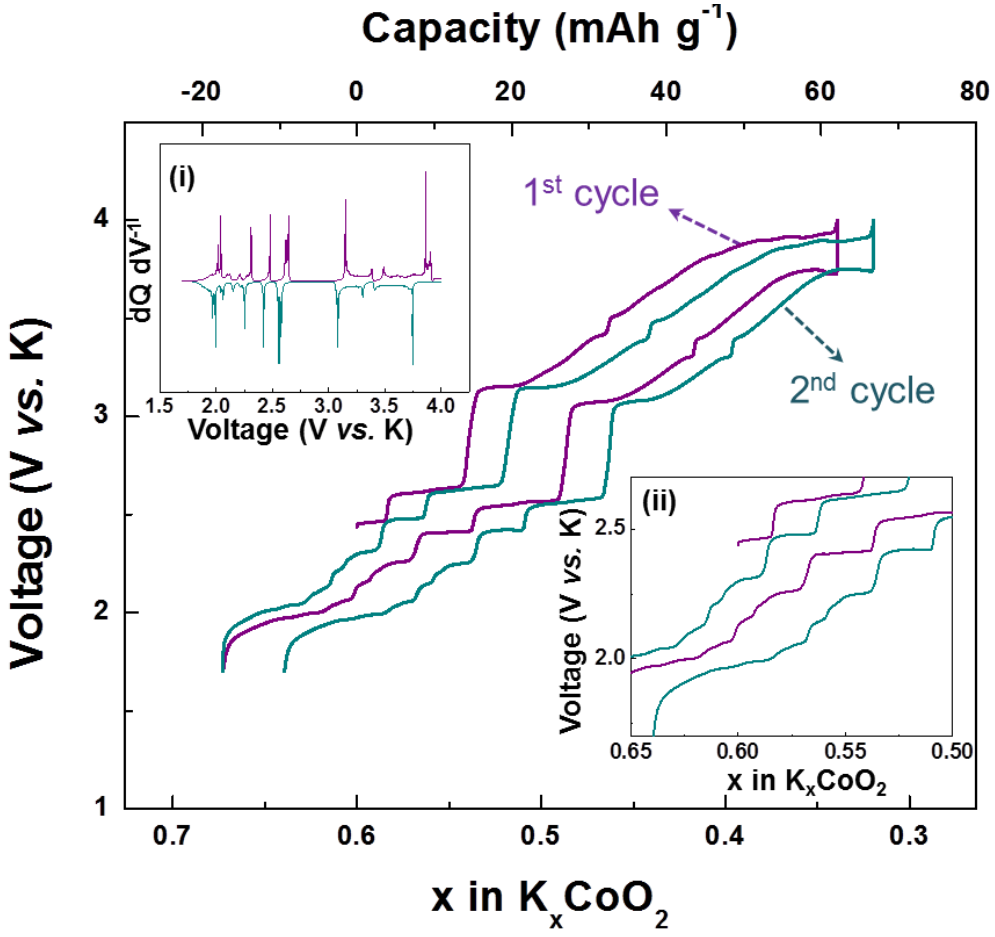

Figure 2. Typical charge/discharge profiles of P2-type $K_{0.6}CoO_2$ at a current rate of 2 mA g^{-1} in the voltage window between 4.0 and 1.7 V *vs.* K/K^+. (inset (i): derivative curve of the second cycle and inset (ii): enlarged charge/discharge curves with K content between 0.5-0.65.)

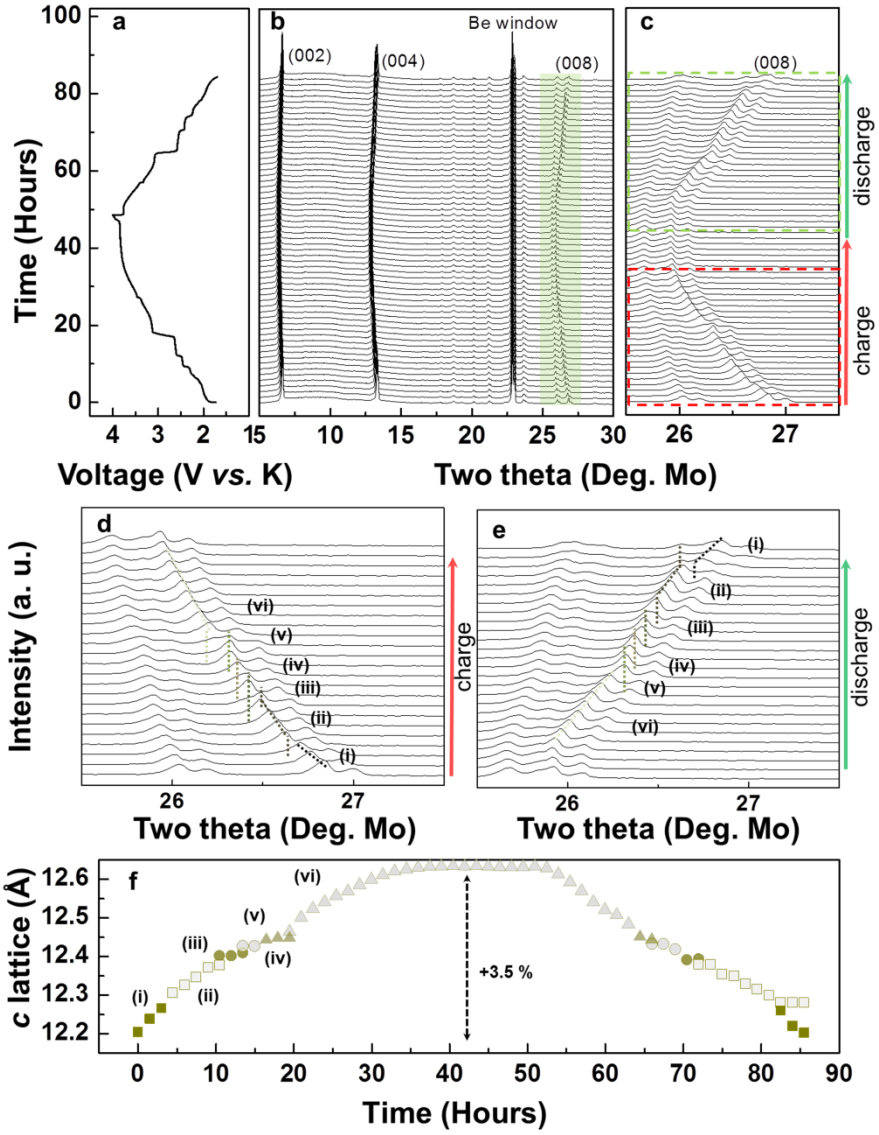

Figure 3. In situ XRD characterization of P2-type $K_{0.6}CoO_2$ upon charge/discharges. a. Typical charge/discharge profiles of P2-type $K_{0.6}CoO_2$ at a current rate of 2 mA g^{-1}. **b.** *In situ* XRD patterns from 15º to 30º. **c.** (008) peaks obtained from *in situ* XRD. Enlarged images of *in situ* XRD patterns upon **d.** charge and **e.** discharge. **f.** *c* lattice parameters calculated from XRD patterns during charge and discharge processes.

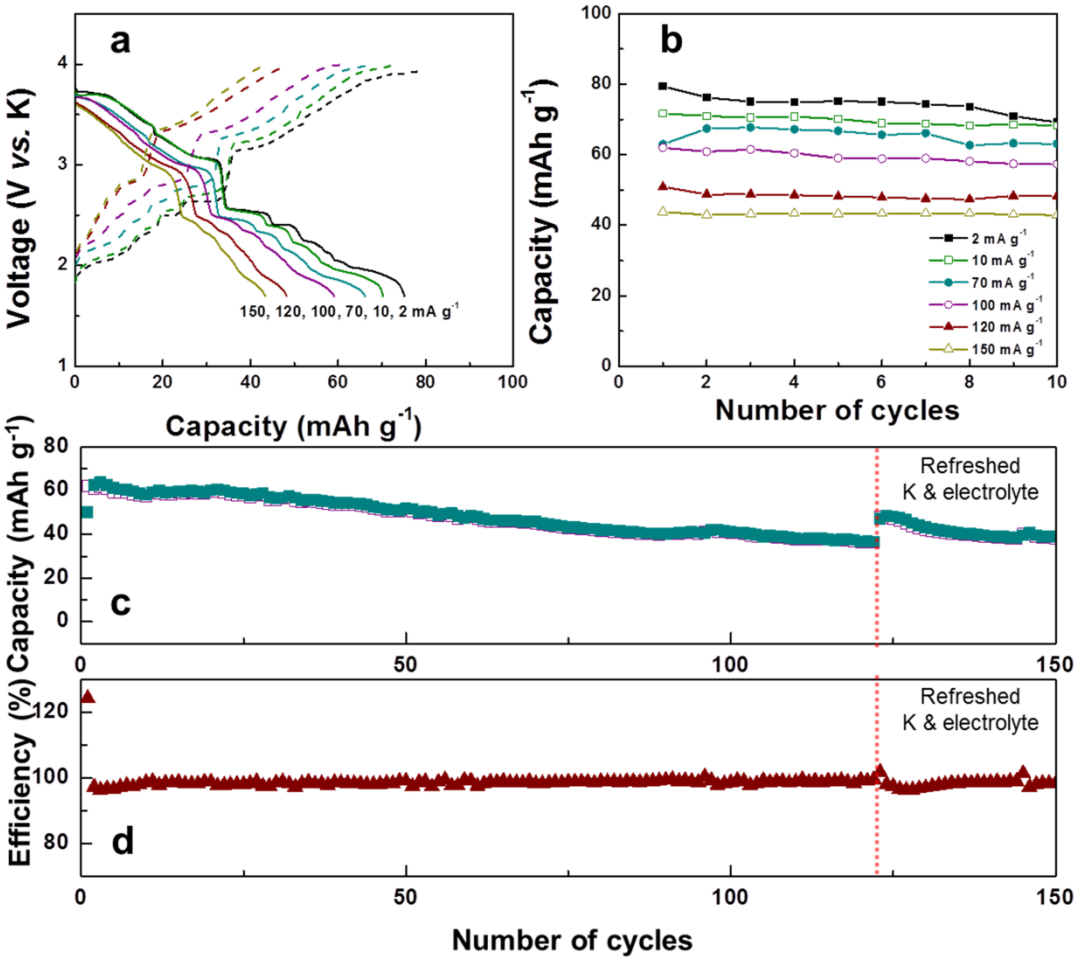

Figure 4. Electrochemical properties of P2-type $K_{0.6}CoO_2$. a. Typical charge/discharge profiles at different rates, and **b.** cycle stability of P2-type $K_{0.6}CoO_2$ at different current rates. **c.** Cycle stability and **d.** coulombic efficiency of P2-type $K_{0.6}CoO_2$ at a current rate of 100 mA g^{-1} in the voltage range of 4.0–1.7 V *vs.* K/K^+.

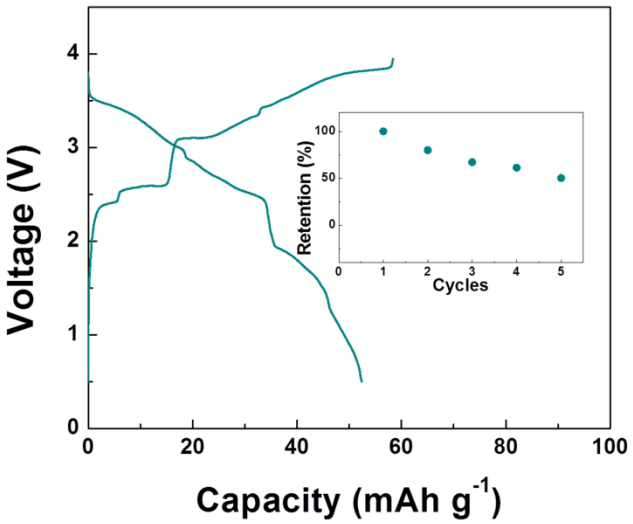

Figure 5. Charge/discharge profile of $K_{0.6}CoO_2$/graphite full cell at a current of 3 mA g^{-1} (inset: capacity retention).

Layered P2-type $K_{0.6}CoO_2$ cathode can accommodate highly reversible K ion intercalation. The K-intercalation in P2-type $K_{0.6}CoO_2$ occurs at high rate, despite the multitude of phase transitions that we observe with *in-situ* X-ray diffraction. The practical feasibility of K-ion batteries is further demonstrated by constructing full cells with a graphite anode.

Keyword potassium, batteries, energy storage, cobalt oxide, cathode

*Haegyeom Kim, Jae Chul Kim, Shou-Hang Bo, Tan Shi, Gerbrand Ceder**

K-ion batteries based on a P2-type $K_{0.6}CoO_2$ cathode